Society For Biomaterials

Microstructure, mechanical property, corrosion behavior, and *in vitro* biocompatibility of Zr–Mo alloys

F. Y. Zhou,[1] B. L. Wang,[1] K. J. Qiu,[1] L. Li,[1] J. P. Lin,[2] H. F. Li,[3] Y. F. Zheng[1,3]

[1]Center for Biomedical Materials and Engineering, Harbin Engineering University, Harbin 150001, China
[2]State Key Laboratory for Advanced Metals and Materials, University of Science and Technology Beijing, Beijing 100083, China
[3]Department of Materials Science and Engineering, College of Engineering, Peking University, Beijing 100871, China

Received 7 April 2012; revised 13 August 2012; accepted 20 August 2012
Published online 10 November 2012 in Wiley Online Library (wileyonlinelibrary.com). DOI: 10.1002/jbm.b.32833

Abstract: In this study, the microstructure, mechanical properties, corrosion behaviors, and *in vitro* biocompatibility of Zr–Mo alloys as a function of Mo content after solution treatment were systemically investigated to assess their potential use in biomedical application. The experimental results indicated that Zr–1Mo alloy mainly consisted of an acicular structure of α' phase, while ω phase formed in Zr–3Mo alloy. In Zr–5Mo alloy, retained β phase and a small amount of precipitated α phase were observed. Only the retained β phase was obtained in Zr–10Mo alloy. Zr–1Mo alloy exhibited the greatest hardness, bending strength, and modulus among all experimental Zr–Mo alloys, while β phase Zr–10Mo alloy had a low modulus. The results of electrochemical corrosion indicated that adding Mo into Zr improved its corrosion resistance which resulted in increasing the thermodynamic stability and passivity of zirconium. The cytotoxicity test suggested that the extracts of the studied Zr–Mo alloys produced no significant deleterious effect to fibroblast cells (L-929) and osteoblast cells (MG 63), indicating an excellent *in vitro* biocompatibility. Based on these facts, certain Zr–Mo alloys potentially suitable for different biomedical applications were proposed. J Biomed Mater Res Part B: Appl Biomater 101B: 237–246, 2013.

Key Words: Zr–Mo alloys, microstructure, mechanical properties, corrosion, cytotoxicity

How to cite this article: Zhou FY, Wang BL, Qiu KJ, Li L, Lin JP, Li HF, Zheng YF. 2013. Microstructure, mechanical property, corrosion behavior, and *in vitro* biocompatibility of Zr–Mo alloys. J Biomed Mater Res Part B 2013:101B:237–246.

INTRODUCTION

The combination of acceptable strength, high corrosion resistance, and good biocompatibility has made zirconium alloys suitable for biomaterials for orthopedic implants.[1–3] Zirconium has been recognized to be nontoxic and nonallergic.[4,5] *In vivo* evidences showed that zirconium implants exhibited good osseointegration and even a higher degree of bone–implant contact than titanium implants.[6,7] By bioactive surface modifications such as NaOH treatment[8] and sol–gel method,[9] a bone-like apatite layer could form on the surface of Zr metal, through which the implant bonds to bone. The ZrO_2 nanotube on Zr metal fabricated by anodization could not only improve functionality and the mineralization of the osteoblast due to its large surface area and unique nanoscaled geometry,[10] but also enhance the forming capability of hydroxyapatite (HA).[11] An ultrafine grained (UFG) Zr with improved mechanical properties and excellent *in vitro* biocompatibility was expected to become a novel biomaterial for surgical implants.[12] In addition, a thin oxide film could spontaneously form on the surface of Zr and its alloys in various electrolytes, which offers them a superior corrosion resistance.[13,14] However, the passive film is not very stable and pitting corrosion easily occurs for Zr and Zr alloys in chloride medium.[14,15] It was suggested that their corrosion resistance would be further improved by alloying[16,17] or surface treatment.[18,19] The oxinium (surface oxidized Zr–2.5Nb alloy) has been commercially used as knee and hip femoral heads in total joint arthroplasty owing to its superior wear resistance.[20,21] Moreover, the surface oxidized zirconium alloy exhibited an excellent anti-bacterial property.[22]

Magnetic resonance imaging (MRI) is widely used as a powerful diagnostic tool in orthopedics and brain surgery.[23] But, MRI diagnosis is inhibited with the presence of metallic

Correspondence to: Y. F. Zheng; e-mail: yfzheng@pku.edu.cn
Contract grant sponsor: State Key Lab of Advanced Metals and Materials; contract grant number: 2011-ZD01
Contract grant sponsor: National Basic Research Program of China (973 Program); contract grant number: 2012CB619102
Contract grant sponsor: National High Technology Research and Development Program of China (863 Program); contract grant numbers: 2011AA030101, 2011AA030103
Contract grant sponsor: National Natural Science Foundation of China; contract grant numbers: 31170909, 51041004
Contract grant sponsor: Research Fund for the Doctoral Program of Higher Education; contract grant number: 20100001110011
Contract grant sponsor: Fundamental Research Funds for the Central Universities; contract grant numbers: HEUCFZ1017, HEUCFR1020
Contract grant sponsor: Natural Science Foundation of Heilongjiang Province; contract grant number: ZD201012

implants in body because they become magnetized in the intense magnetic field of the MRI instrument, which causes artifacts on the image.[23,24] So devices with low magnetic susceptibility (χ) are required. Compared to stainless steel, Co–Cr alloy, and titanium, zirconium has lower magnetic susceptibility and is more suitable for surgery performed in an MRI circumstance.[25] It has been reported that the magnetic susceptibility strongly depends on the phase constitutions of Zr–Mo alloys[25,26] and Zr–Nb alloys.[27] The magnetic susceptibility of different phases decreased in following sequence, $\chi_\beta > \chi_{\alpha'} > \chi_\omega$ and the alloys consisting of α' phase were proposed as candidates for medical devices used under MRI.

Molybdenum (Mo) also has less magnetic susceptibility,[25] low toxicity,[28] and is an effective strengthening element for zirconium.[29] However, there has been no systematic investigation on corrosion behaviors of Zr–Mo alloys in simulated physiological media. Meanwhile, *in vitro* biocompatibility of Zr–Mo alloys has been scarcely reported. In this study, alloy solution treatment has been adopted to obtain the various phases of Zr–Mo alloys after quenching. This article aims to precisely evaluate the effects of Mo content on the microstructure, mechanical properties, corrosion behaviors, and *in vitro* biocompatibility of Zr–Mo alloys.

MATERIALS AND METHODS

Alloys preparation

The binary Zr–Mo alloys with different compositions (0, 1, 3, 5, and 10 wt % of Mo) were prepared from zirconium wire (99.9%) and Mo foil (99.9%) in a non-consumable arc melting furnace under an Ar atmosphere. The alloy ingots were remelted six times by inversion to promote the homogeneity of the alloying element. The obtained ingots were then hot-rolled to $\sim$1.5 mm thick sheets at 800°C. The samples were prepared by electro-discharge machining from the rolled plates and then they were solution treated at 950°C for 30 min, followed by quenching in iced water. In addition, pure titanium (grade 2, TA2), Ti–6Al–4V alloy (TC4), AISI 304 stainless steel (304 SS), and AISI 316L stainless steel (316L SS) were obtained and tested as reference materials.

Microstructure characterization

X-ray diffractometer (XRD, Philips X'Pert Pro, Holland) with a Ni filtered Cu Kα radiation was employed to analyze the phase constitution of the experimental Zr–Mo alloys. The microstructure of the alloys was examined using transmission electron microscope (TEM, JEM-2100, JEOL, Japan). The TEM specimens were prepared by a twin-jet polisher with a solution of 10% $HClO_3$ and 90% C_2H_5OH at 20–35 V and 223 K, after mechanically thinning to about 60 μm.

Mechanical properties measurement

Three-point bending test was performed on a mechanical tester (Instron5969, America) with a crosshead speed of 0.25 mm/min at room temperature. The pre-set maximum deflection at middle span was 8 mm. The bending strength is determined using the equation,[30] $\sigma = 3PL/2bh^2$, where σ is the bending strength (MPa), P is the load (N), L is the span length (mm), b and h are the width (mm) and the thickness (mm) of the specimens, respectively. In this process, the span length was 30 mm, and the dimension of test specimen was 3 mm (width) $\times$ 1 mm (thickness). The modulus of elasticity (E) in bending is calculated from the equation,[30] $E = L^3\Delta P/4bh^3\Delta\delta$, where ΔP is the load increment and $\Delta\delta$ is the deflection increment at middle span. The $\Delta P/\Delta\delta$ is determined from the load increment and the corresponding deflection increment on the straight line of the stress-deflection profile. The average bending strength and modulus were obtained from three tests for each alloy.

In addition, a digital hardness tester (HVS-1000, China) was employed to examine the microhardness of the experimental Zr–Mo alloys. A load of 500 g was loaded and dwelt for 15 s, repeating six times in different positions of each sample to get an average value.

Electrochemical measurement

The electrochemical corrosion measurements of Zr–Mo alloys were performed with a conventional three-electrode cell, consisting of a working electrode (test specimen), a platinum electrode, and a saturated calomel electrode (SCE) as reference electrode. Prior to testing, the samples were wet-ground to 2000 grit, and were later cleaned in acetone, ethanol, and de-ionized water in an ultrasonic bath. The electrolyte used to simulate human body condition was simulated body fluid (SBF), with ion concentrations nearly equal to those of human blood plasma.[31] Fresh prepared SBF solution with pH = 7.4 was used for each test, which was conducted at 37°C in a water bath. The open-circuit potential (OCP) measurement was maintained up to 7200 s after sample immersed in SBF solution. The potentiodynamic polarization measurement was conducted from -1.0 V to 1.5 V (vs. SCE) at a scan rate of 1 mV/s. The morphology of the corroded sample was examined by scanning electron microscopy (SEM, S4800, Hitachi, Japan).

Cytotoxicity test

The cytotoxicity test was carried out based on ISO 10993-5:1999.[32] Murine fibroblast cells (L-929) and human osteosarcoma cells (MG 63) were chosen to evaluate the cytotoxicity of Zr–Mo alloys in their extracts. L-929 cells and MG 63 cells were cultured in Dulbecco's modified Eagle's medium (DMEM) and Minimum Essential medium (MEM), respectively. Each medium was supplemented 10% fetal bovine serum (FBS), 100 U/mL penicillin, and 100 μg/mL streptomycin. In this indirect test, extracts of the studied materials were obtained using serum-free medium as the extraction medium. The samples were wet-ground to 2000 grit, cleaned, dried, and then sterilized by UV–light radiation for 12 h. For each 3 cm^2 of material (surface area), 1 mL of culture medium was used and then incubated for 72 h. The medium (DMEM for L-929 cells and MEM for MG 63 cells) was used as a negative control, and the medium containing 10% dimethylsulfoxide (DMSO) as a positive control. All the culturing was kept at 37°C in a humidified atmosphere of 5% CO_2 in an incubator. In addition, the amount of metal

ions released into culture media (extracts) was measured by the inductively coupled plasma atomic emission spectrometry (Profile ICP-AES, Leeman, America).

Cells were seeded in each well of 96-well cell culture plates at a density of 5×10^3 cells/100 μL medium and incubated for 24 h to allow attachment. After that, the culture medium in each well was substituted by the extract obtained from the material, and then incubated for 1, 2, and 4 days. After that 10 μL 3-(4, 5-dimethylthiazol-2-yl)-2,5-diphenyltetrazolium bromide (MTT, Sigma-Aldrich, America) was added to each well, followed by 4 h incubation at 37°C in darkness. Then 100 μL formazan solubilization solution (10% sodium dodecyl sulfate (SDS) in 0.01*M* HCl) was added overnight in the incubator. The spectrophotometrical absorbance of the product in each well was measured by microplate reader (Bio-RAD680, America) at 570 nm with a reference wavelength of 630 nm.

Statistical analysis

Statistical analysis was performed with SPSS 18.0 software. Differences between groups were analyzed using one-way ANOVA, followed by Tukey's test. $p < 0.05$ was considered statistically significant.

RESULTS

Microstructure

Figure 1(a) shows XRD patterns of pure Zr and binary Zr–Mo alloy samples at room temperature. The results indicated that the phase constitution of solution-treated Zr–Mo alloys strongly depended on the composition (Mo content). As indicated in Figure 1(a), only the peaks originated from α phase (hexagonal close packed structure) were observed in pure zirconium. Zr–1Mo alloy was found to mainly consist of α phase and a small amount of β phase (body centered cubic structure). Both Zr–3Mo alloy and Zr–5Mo alloy consisted of duplex phases, α and β. It was noteworthy that the β (211) peak ($2\theta = 57°$) showed an increasing intensity with the increase of Mo content. When the Mo content increased to 10 wt %, only the retained β phase was observed. The lattice parameter (a) of β phase (calculating from the β (200) peak) as a function of Mo content is shown in Figure 1(b). The lattice parameter remained almost constant when Mo content was lower than 3 wt % and markedly decreased when Mo content further increased up to 10 wt %. The decrease in lattice parameter of β phase could be explained by the formation of the substitutional solid solution (cubic lattice) when alloying Mo to Zr. Due to smaller atom radius of Mo than Zr,[33] the addition of Mo to Zr caused the parameter of the cubic lattice to decrease. Moreover, the result indicated that more Mo dissolved into β phase with the increasing of Mo content.

Figure 2 shows TEM micrographs of solution-treated Zr–Mo alloys. As shown in Figure 2(a), the bright field image of Zr–1Mo alloy revealed the presence of acicular plates along different direction. The selected-area electron diffraction (SAED) pattern presented α phase (hexagonal close packed) reflection. Therefore, the acicular structure corresponded to α′ martensite, which was formed by the

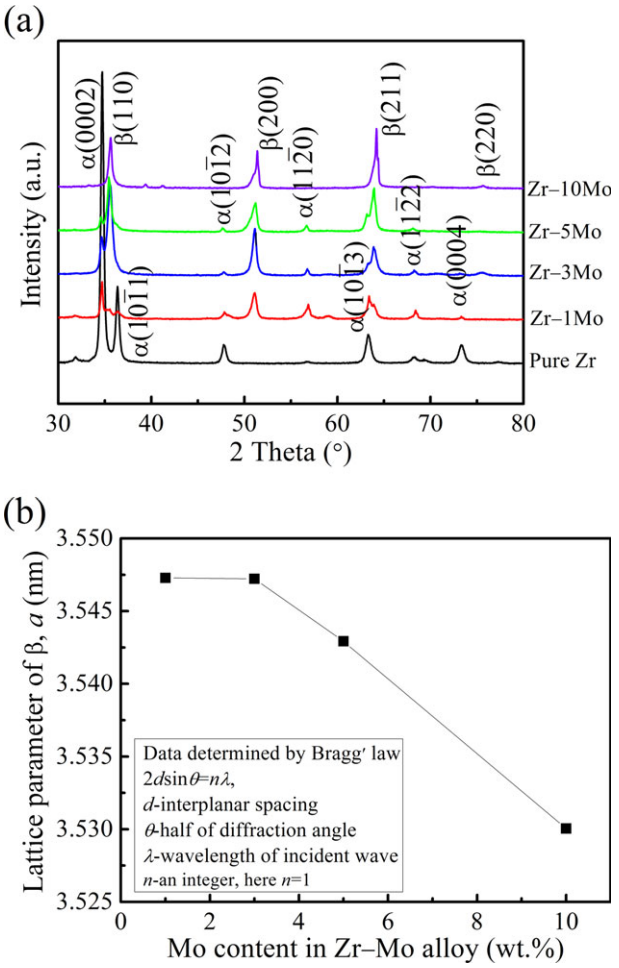

FIGURE 1. (a) XRD profiles of pure Zr and Zr–Mo alloys and (b) lattice parameter of β phase of various Zr–Mo alloys. [Color figure can be viewed in the online issue, which is available at wileyonlinelibrary.com.]

martensitic transformation during cooling. Several coarse grains were observed in Zr–3Mo alloy and, in the grains, the homogeneous rugged morphology could be seen, as shown in Figure 2(b). The presence of ω originating in the β was confirmed in the diffraction pattern. Moreover, via careful observation, small noodle-shaped precipitate could be found in the matrix, which was proved to be of hexagonal structure (α phase) by the SAED. So the SAED patterns of Zr–3Mo alloy indicated that its structure consisted of β, ω, and α. For Zr–5Mo alloy, the bright-field image showed that the straight plate precipitate with a width of around 100–120 nm was present in the matrix. The SAED pattern from this precipitate was consistent with α phase. The matrix was β phase and ω phase could not be found. In Zr–10Mo alloy, only β phase was confirmed according to the bright field image and SAED pattern with zone axis $[001]_\beta$.

Mechanical properties

The mechanical properties of Zr–Mo alloys together with TC4 and 304 SS as controls are shown in Figure 3. As shown in Figure 3(a), all studied Zr–Mo alloys exhibited a significantly higher strength than pure Zr ($p < 0.05$). The

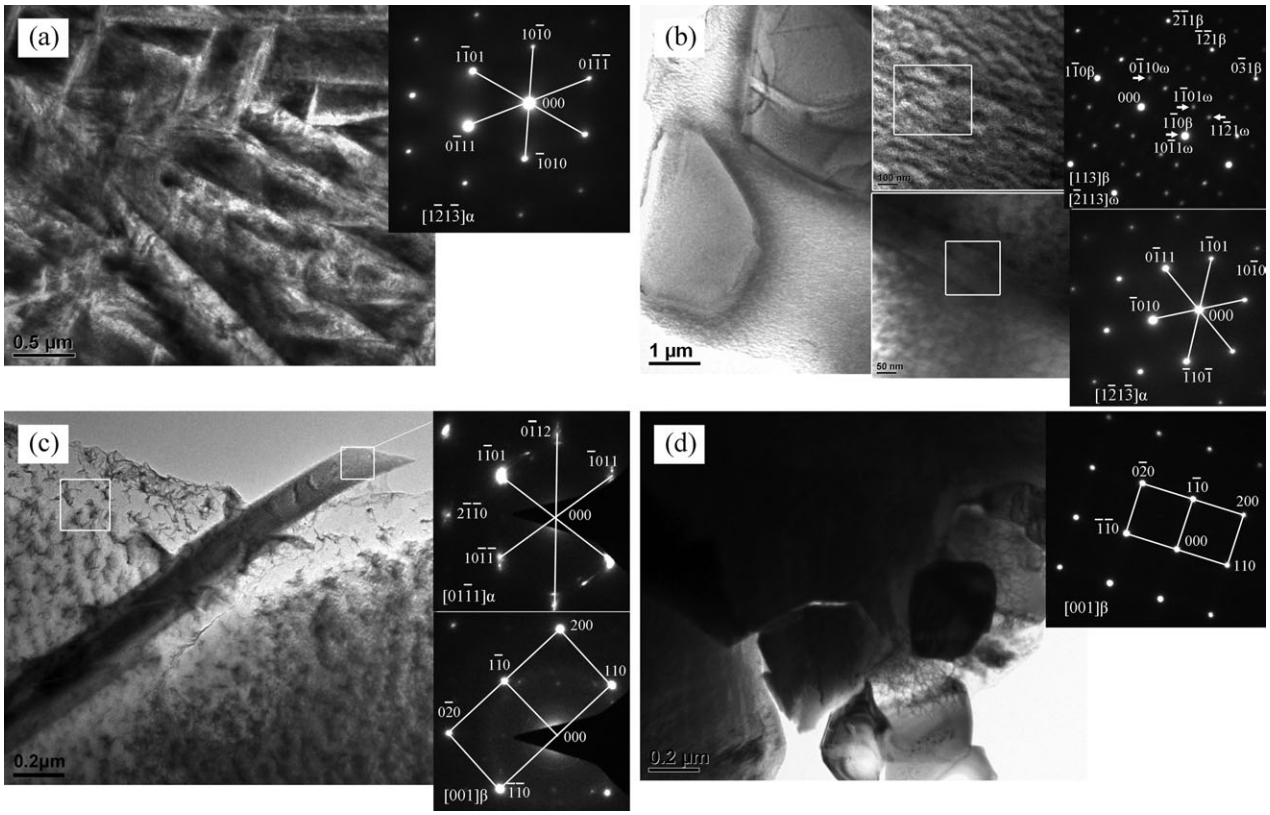

FIGURE 2. TEM micrographs of Zr–Mo alloys including bright field images and SAED patterns: (a) Zr–1Mo alloy, (b) Zr–3Mo alloy, (c) Zr–5Mo alloy, and (d) Zr–10Mo alloy.

bending strengths of Zr–Mo alloys decreased with the increase of Mo content, but there was an invert for Zr–10Mo alloy. The α′ phase dominated Zr–1Mo alloy had the highest bending strength (1780 MPa) among pure Zr and Zr–Mo alloys, which had a similar bending strength to TC4. The bending modulus of pure Zr and Zr–Mo alloys are present in Figure 3(b). Zr–Mo alloys possessed lower elastic modulus in comparison with TC4 and 304 SS ($p < 0.05$). The bending modulus of pure Zr (99 GPa) was slightly higher than Zr–1Mo alloy. Moreover, the bending modulus decreased with the increasing of Mo content for Zr–1Mo alloy (98 GPa), Zr–3Mo alloy (95 GPa), and Zr–5Mo alloy (72 GPa). This variation was attributed to the fact that the volume fraction of β phase increased with an increase of Mo content in Zr–Mo alloys and β phase had a lower modulus than α phase and α′ phase. Zr–10Mo alloy had a similar bending modulus to Zr–5Mo alloy. Previous work by Ho et al.[34] indicated that a bending strength/modulus ratio (×1000) was used to assess the feasibility of implanted materials. As indicated in Figure 3(c), Zr–1Mo alloy and Zr–5Mo alloy exhibited higher bending strength/modulus ratio compared to TC4 and 304 SS (as high as 18.04 and 18.01, respectively), showing their potential for use as new implants.

The variation in microhardness with the amount of Mo content had a similar trend in bending strength, as shown in Figure 3(d). It could be observed that all present Zr–Mo alloys had much higher hardness than pure Zr ($p < 0.05$). The hardness of Zr–Mo alloys decreased with an increasing Mo content from 424 Vickers hardness (HV) (α′ phase dominated Zr–1Mo alloy) to 323 HV (β phase Zr–10Mo alloy). This result suggested that cubic β phase appeared to be softer than hexagonal α′ phase in Zr–Mo alloys, which was similar to the cast Zr–Ti alloy reported in a previous study.[30]

Corrosion behavior

OCP is the potential at which the metal reaches equilibrium with the liquid environment.[35] Figure 4 shows OCP vs. time curves of pure Zr and Zr–Mo alloys together with TC4 and 316L SS in SBF solution. The OCPs of TC4 and 316L SS stabilized at nobler values in comparison with pure Zr and studied Zr–Mo alloys in SBF medium. It could be found that OCPs changed slowly toward noble potentials for pure Zr and all experimental Zr–Mo alloys during the whole immersion process. This fact implied that the passive film spontaneously formed on surface of pure Zr and Zr–Mo alloys, which was resistant to metal dissolution into SBF solution. By comparing the OCP values, Zr–Mo alloys possessed more positive potentials than pure Zr, and Zr–10Mo alloy had the most positive value. The results indicated that the addition of Mo made the spontaneous passive film on the metallic surface more stable thermodynamically, thus rendering these alloys a lower corroding tendency compared to pure Zr.

For further understanding of the effect of Mo addition on the corrosion resistance of Zr–Mo alloys in physiological

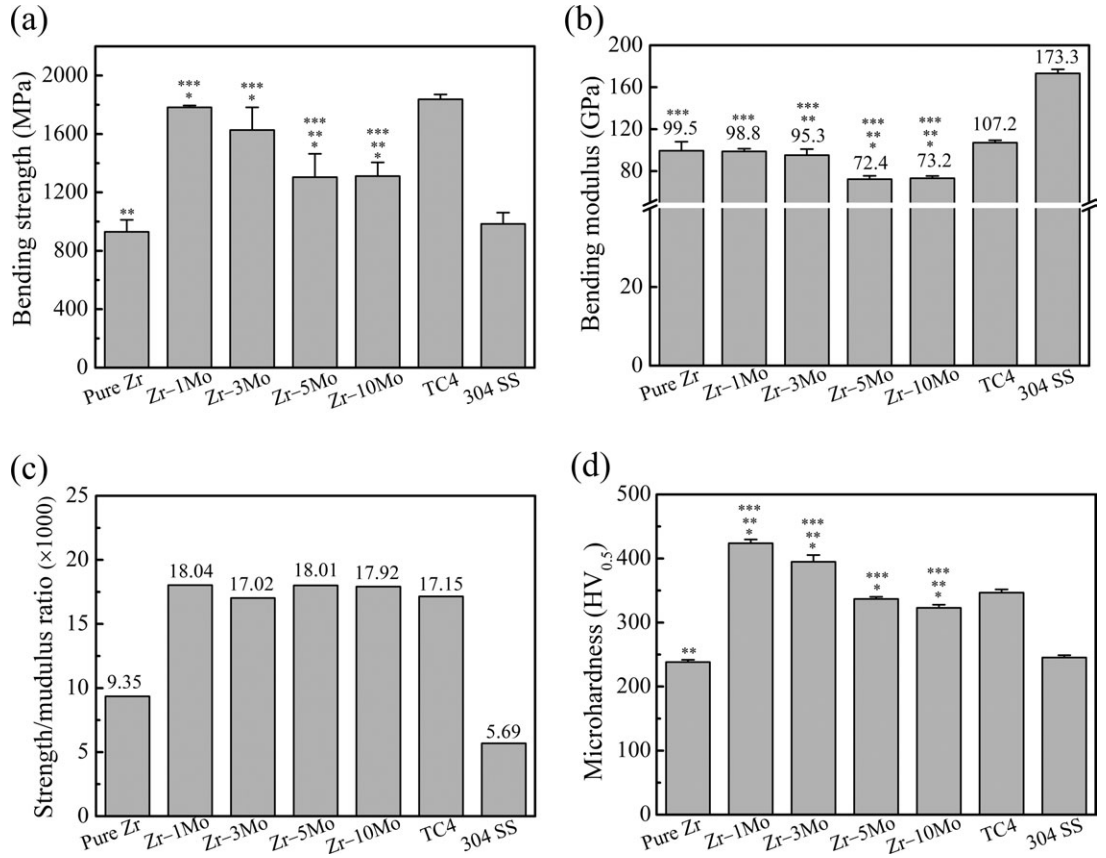

FIGURE 3. Mechanical properties of pure Zr and Zr–Mo alloys together with TC4 and 304 SS: (a) bending strength, (b) bending modulus, (c) strength/ modulus ratio, and (d) microhardness. * indicates $p < 0.05$ when compared with pure Zr. **indicates $p < 0.05$ when compared with TC4. *** indicates $p < 0.05$ when compared with 304 SS.

medium, the potentiodynamic polarization scan was carried out in the potential range of −1.0 to 1.5 V (vs. SCE), and the results are shown in Figure 5. Stainless steel, Zr alloys, and Ti alloy displayed different polarization characteristics. For 316L SS, the cathodic branch moved to higher current density region and the breakdown potential was lower than those of Zr alloys and Ti–6Al–4V alloy. A wider passive region was observed on the anodic polarization curve of

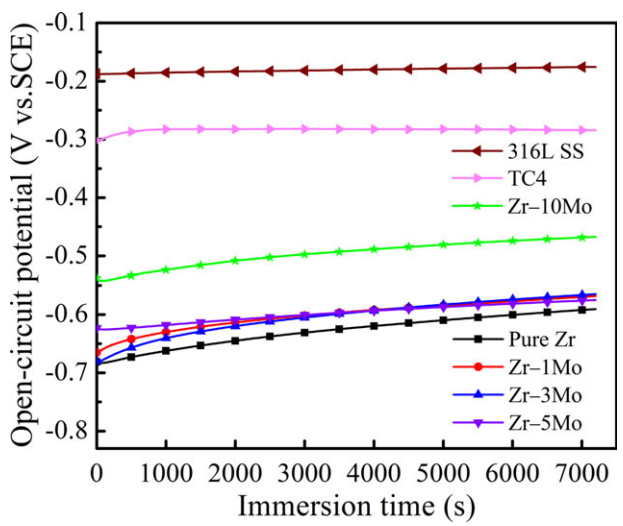

FIGURE 4. OCP vs. time curves of pure Zr and Zr–Mo alloys together with TC4 and 316L SS in SBF solution. [Color figure can be viewed in the online issue, which is available at wileyonlinelibrary.com.]

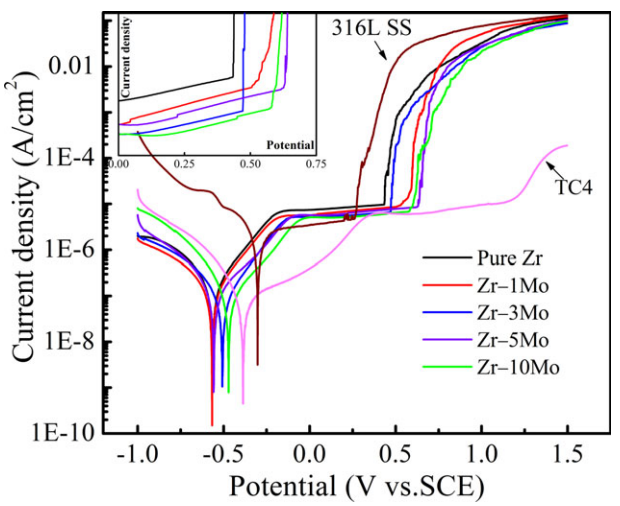

FIGURE 5. Potentiodynamic polarization curves of pure Zr and Zr–Mo alloys together with TC4 and 316L SS in SBF solution. [Color figure can be viewed in the online issue, which is available at wileyonlinelibrary.com.]

TABLE I. Corrosion Parameters of Pure Zr, Zr–Mo Alloys, TC4 and 316L Stainless Steel Obtained from Polarization Curves

Samples	E_{corr} (V)	I_{corr} (10^{-7} A/cm^2)	E_{tran} (V)
Pure Zr	−0.542 ± 0.022	1.612 ± 0.963	0.415 ± 0.036
Zr–1Mo	−0.591 ± 0.071	1.259 ± 0.485	0.521 ± 0.262
Zr–3Mo	−0.565 ± 0.048	0.667 ± 0.292	0.512 ± 0.123
Zr–5Mo	−0.577 ± 0.017	1.413 ± 0.543	0.629 ± 0.029
Zr–10Mo	−0.481 ± 0.026	1.536 ± 0.378	0.583 ± 0.152
TC4	−0.391 ± 0.041	0.768 ± 0.042	1.194 ± 0.017
316L SS	−0.299 ± 0.018	10.33 ± 2.08	0.290 ± 0.022

Ti–6Al–4V alloy, which had the highest breakdown potential. Pure Zr and studied Zr–Mo alloys showed quite similar polarization behavior and the shape of polarization curves revealed the characteristic of a typical valve metal (valve metals,[14,36] such as Ti, Zr, Ta, Nb, and W, are usually covered by a thin passive film, which protects the metal from dissolution; at a rather high potential, the breakdown of passive film may occur). The corrosion current density (I_{corr}) and corrosion potential (E_{corr}) were estimated by Tafel extrapolation method using both cathodic and anodic branches of the polarization curve. The average values of E_{corr} and I_{corr} are listed in Table I. The corrosion current densities of studied Zr–Mo alloys were similar to that of Ti–6Al–4V alloy, and far lower than that of 316L SS. With addition of Mo, the corrosion current densities of Zr–Mo alloys decreased and Zr–3Mo alloy had the lowest value, which suggested that the corrosion resistance of pure Zr improved after alloying. A passive region (stabilization in current density) was observed on the anodic branch of polarization curve before transpassivation occurrence, which indicated that the stable and protective film was formed on the surface of the sample. The passive current densities of all test alloy samples were around 5–10 μA/cm^2 and the values decreased from pure Zr to Zr–10Mo alloy, which indicated that addition of Mo increased the passivity of Zr (the detailed view is shown in Figure 5). It implied that mixed oxide film offered a better protection than the pure Zr-oxide passive film and it became more stable with the increase of Mo content for Zr–Mo alloys. At more positive potential, the passive films broke down and the current densities increased rapidly. The breakdown potentials for pure Zr and Zr–Mo alloys are listed in Table I. Comparing with pure Zr, the breakdown potentials for the studied Zr–Mo alloys increased regardless of the Mo content of the alloys. Hence, the addition of Mo enhanced pitting resistance of Zr in SBF solution. It was also clear from the breakdown potentials that with the increase of Mo content, the stability of protective films increased and consequently, the pitting resistance increased for these binary Zr–Mo alloys (there was an invert for Zr–10Mo alloy). TC4 showed a higher breakdown potential compared to Zr–Mo alloys, which suggested that Ti-oxide was more stable with respect to Zr-oxide at high potentials (higher than 0.4 V). 316L SS had the lowest breakdown potential (0.290 V vs. SCE). The typical surface morphology of Zr–10Mo alloy after potentiodynamic polarization is shown in Figure 6. The morphologies of corroded surfaces of test samples are very similar, so other images are not given here. Distinct pits randomly distributed on the corroded sample's surface, which confirmed that pure Zr and all Zr–Mo alloys suffered pitting corrosion after potentiodynamic polarization up to 1.5 V (vs. SCE). In general, the addition of Mo significantly enhanced the corrosion resistance of Zr. Moreover, with the increase of Mo content, the corrosion resistance of Zr–Mo alloys further increased as indicated in the decrease in passive current densities and the increase in breakdown potentials (except for Zr–10Mo alloy).

Evaluation of cytotoxicity

In order to examine substances released into the culture medium by tested material, the amount of metallic ions in extracts was measured by the ICP-AES. All metal ions (Zr, Mo, and Ti) were not detectable, namely under the minimal detection limit of the machine (0.001 μg/mL). Figure 7(a) illustrates the relative viability of murine fibroblast cells (L-929) expressed as a percentage of the viability of cells grown in the negative control after culturing in Ti (TA2), pure Zr, and various Zr–Mo alloys extraction media for 1, 2,

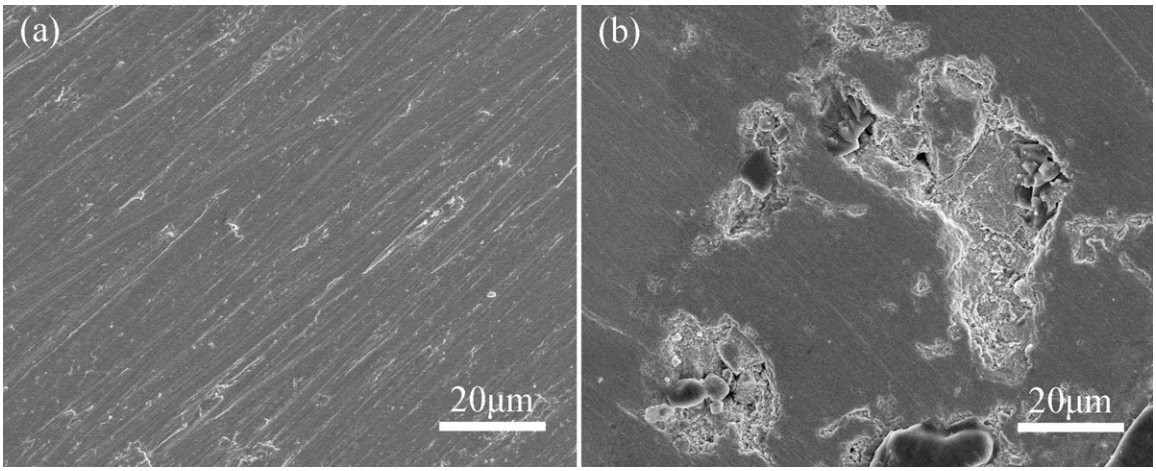

FIGURE 6. SEM images of the surface of Zr–10Mo alloy: (a) before and (b) after potentiodynamic polarization.

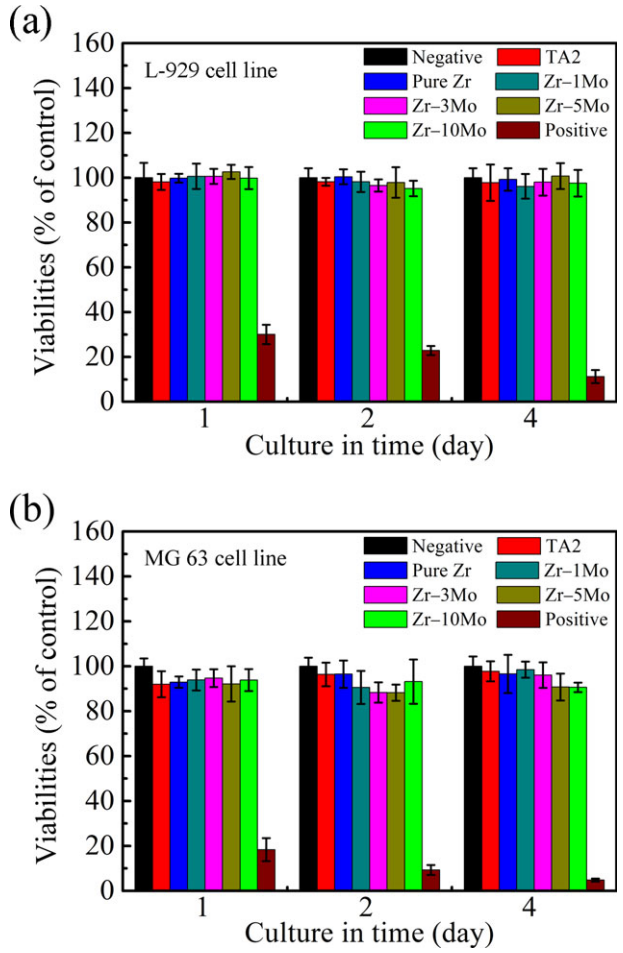

FIGURE 7. Cell viability expressed as a percentage of the viability of cells in the negative control after 1, 2, and 4 days culture in Ti, pure Zr and Zr–Mo alloys extraction media: (a) L-929 cell line and (b) MG 63 cell line. [Color figure can be viewed in the online issue, which is available at wileyonlinelibrary.com.]

and 4 days, respectively. It could be seen that the cell viability in extracts of pure Zr and Zr–Mo alloys was almost the same as in those of negative group and Ti regardless of culture time. It suggested that the extracts of pure Zr and Zr–Mo alloys samples showed no toxicity to L-929 cells. Figure 7(b) shows the relative viability of the human osteosarcoma cells (MG 63). After 1 day culture, the cell viabilities of pure Zr and Zr–Mo alloys were almost the same as that of Ti, but lower than that of negative group. The extracts of Zr–1Mo alloy, Zr–3Mo alloy, and Zr–5Mo alloy showed slight reduced values of cell viability compared to that of Ti and the cell viability of Zr–3Mo alloy was lowest (88% of control) in 2 days culture. After a prolonged culturing period (4 days), MG 63 cell viabilities decreased with the increase of Mo content for Zr–Mo alloys, but the lowest value of cell viability was higher than 90% (of the control). Although Zr–Mo alloys displayed reduced cell viability in comparison with the negative control, but the value of cell viability was still above 88%, approximately equivalent to level of non-cytotoxicity. In conclusion, the indirect cytotoxicity test showed that the studied Zr–Mo alloys did not release any toxic component which inhibited the growth and proliferation of fibroblast cells and osteoblast cells, indicating a good *in vitro* biocompatibility.

DISCUSSIONS

Effect of Mo content on microstructure and mechanical properties of Zr–Mo alloys

XRD analysis and TEM observation revealed that Zr–Mo alloys underwent a variety of phase transformations and several metastable phases including α′ (martensite), ω, and retained β were formed during quenching. In Zr–1Mo alloy, β phase transformed to martensite, but the transformation was not complete and a small amount of β phase remained after treating (XRD result). When the Mo content increased up to 3 wt %, β phase started to transform to ω phase but this transformation was still incomplete. The previous investigations,[25,37] on non-equilibrium transformations of Zr–Mo system, showed that when the Mo content was less than about 3 wt %, the martensite start temperature (M_s) was higher than ω start temperature (ω_s) so α′ martensite formed first, followed by the forming of ω phase. With the Mo content exceeding 3 wt %, ω_s was higher than M_s, and the ω transformation prevailed over the martensite transformation during cooling. In this study, the presence of α′ phase in Zr–1Mo alloy and ω phase in Zr–3Mo alloy confirmed these non-equilibrium transformations. Moreover, small precipitate of needle-shaped α phase in the matrix confirmed that β→α transformation had taken place. This result was also in accordance with Suyalatu study.[26] In as-quenched Zr–5Mo alloy, these non-equilibrium transformations (martensitic transformation and ω transformation) had been suppressed. For Zr–10Mo alloy, β phase was fully retained and it was reasonably inferred that β phase could be fully stabilized beyond 10 wt % Mo for Zr–Mo alloy.

Mo content had significant influence on the microstructure of Zr–Mo alloys, which consequently affected their deformation behavior and mechanical properties. In fact, both slip and twinning could take place for hexagonal close-packed Zr during plastic deformation.[38] Three-point bending test has been performed to evaluate the mechanical properties of implanted metals or alloys, such as Ti–Nb alloys[39] and Ti–Zr alloys.[40] In fact, orthopedic implants, as structural material, usually subject to load in tension, compression, bending, shear, torsion, or a combination of these modes. In total hip replacement, femoral component of the prosthesis is loaded both axially and in bending, and the near one-third region subjects to the maximum bending.[41,42] In the present article, for the Zr–Mo alloys, the increase in strength was mainly attributed to the solid solution strengthening by alloying with Mo. Zr–3Mo alloy consisted of ω phase, but it was recognized as hard and brittle.[27] The presence of ω phase in alloy was unfavorable for plastic deformation. It was worth noting that α′ phase had higher hardness, bending strength and modulus compared to β phase. A similar result was obtained in as-cast Zr–Ti alloys[30] and Ti–Nb alloys.[39] Zr–1Mo alloy exhibited a high hardness (close to CoCr alloy, 4.28 GPa[43]) and bending strength (similar to TC4). Additionally, it is well known that the mismatch

between bone stiffness and implant stiffness is a significant factor in determining stress shielding, which leads to the loosening of the implant and refracturing of the bone.[44] It is essential to use implant materials with lower elastic modulus (closer to that of natural bone, 10–30 GPa). Compared to Ti–6Al–4V alloy (107.2 GPa) and 304 biomedical stainless steel (173.3GPa), Zr–10Mo alloy (or Zr–5Mo alloy) showed much lower elastic modulus ($p < 0.05$), so they may be promising candidates for new implants in terms of relatively low elastic modulus.

Effect of Mo content on bio-corrosion behaviors of Zr–Mo alloys

The general conclusion of the electrochemical corrosion study was that the alloying of Mo improved the corrosion resistance of pure Zr. The corrosion resistance of Zr–Mo alloys in SBF medium was better than that of AISI 316L stainless steel and was similar to that of Ti–6Al–4V alloy (corrosion current density). Pure Zr and Zr–Mo alloys underwent spontaneous passivation and passive film formed on the metallic surface (OCP results). The corrosion performance of Zr alloys strongly depended on its composition, structure, and environment. The previous corrosion studies[13,16,45] clearly indicated that when adding Ti, Nb, Ta to pure Zr, its corrosion performance improved but adding Hf lowered its corrosion resistance. In addition, the growth and stability of the oxide film on Zr and its alloys were much affected with the presence of chloride ions.[46] The passive film was easily attacked due to the Cl^- migration toward and into the oxide film, which caused pitting.[15] Zr–Mo alloys in this study exhibited better corrosion resistance than pure Zr. It was previously proved that the corrosion resistance of Ti–Mo alloys was improved with the addition of Mo, which was attributed to the passive film formation of mixed TiO_2 and MoO_3 oxides.[47,48] Similarly, it was reasonably inferred that a mixture of Zr-oxide and Mo-oxide generated on the metallic surface, which was responsible for the high corrosion resistance of the studied Zr–Mo alloys. Besides, the mixed passive film consisting of Zr- and Mo-oxides was more stable than single passive film ZrO_2. Pitting corrosion occurred after potentiodynamic polarization up to 1.5 V (vs. SCE) for pure Zr and all studied Zr–Mo alloys (SEM observation). It is necessary for the implanted metals to remain at the passive state in body. Therefore, the breakdown potential of the passive film on a metallic implant is required to be higher than the body potential. It was suggested that the body potential corresponded to the redox potential of the body fluid with value of 0.4–0.5 V.[49] In this study, the breakdown potentials of passive films on Zr–Mo alloys were higher than the redox potential, making them promising materials for new implants in terms of pitting resistance.

Biocompatibility of Zr–Mo alloys and their promises as medical devices

Zr is known to be nontoxic and biocompatible as a stable oxide film is formed on its surface, which can effectively inhibit the releasing of metal ions. Meanwhile, the oxide itself shows bio-inertness and low solubility.[12,50,51] Mo is an essential trace element and the 150–500 μg/day level was estimated as adequate and safe for adults.[52] Based on previous cytotoxicity and biocompatibility studies of metals, Mo was classified as a low cytotoxic and safe element for living body.[28,53] Through animal test, Mo was found in the kidney, liver, and spleen after mandibular implants of Co–Cr–Mo alloy implanting in rabbits for 2 years.[54] In the present study, the amount of Zr and Mo ions released into the culture medium was less than 0.001 μg/mL, which was approximately equivalent to 10^{-5} m*M* (the atomic weight of Zr or Mo ≈100). Early studies demonstrated that below 0.01 m*M*, neither Zr nor Mo was toxic to osteoblasts and fibroblasts.[5,55] In addition, the biocompatibility of Zr–Mo alloys was primarily evaluated by culturing L-929 cells and MG 63 cells in their extraction media and positive results were obtained, indicating an excellent *in vitro* biocompatibility.

Zr–Mo alloys showed a lower magnetic susceptibility than other biomedical metal or alloys (such as Co–Cr–Mo alloy, CP Ti and Ti–6Al–4V alloy). Among various Zr–Mo alloys, Zr–(0.5–1) Mo alloys consisting of the α′ phase were proposed as the best candidates for medical devices used under MRI.[25] Furthermore, in this work, Zr–1Mo alloy exhibited higher hardness, bending strength, and modulus in comparison with other Zr–Mo alloys, which implied high resistance to plastic deformation and wear. Additionally, the β type Zr–Mo alloy displayed a lower modulus in comparison with TC4 and 304 SS, showing a promising potential for new orthopedic implants from the viewpoint of relatively low elastic modulus. Besides, Zr–Mo alloys with higher Mo content exhibited a better pitting resistance than those with low Mo content. In addition, the magnetic susceptibility of β-Zr–Mo alloy was still lower than that of CP Ti and Ti–6Al–4V alloy,[25] indicating MRI compatible as well.

CONCLUSIONS

The microstructure, mechanical properties, corrosion behavior, and *in vitro* biocompatibility of Zr–Mo alloys after solution treating were investigated to explore their potential use in orthopedic application. The alloying element Mo had significant influence on the microstructure of Zr–Mo alloys. The α′ phase with an acicular structure was dominant in Zr–1Mo alloy, while β and ω phases predominantly existed in Zr–3Mo alloy. For Zr–5Mo alloy, a lot of β phase retained and a small amount of α precipitated in the β matrix, while β phase was fully retained in Zr–10Mo alloy. Zr–1Mo alloy exhibited higher hardness, bending strength, and modulus than other Zr–Mo alloys. The β type Zr–Mo alloys showed low bending modulus. The results of electrochemical corrosion suggested that alloying of Mo improved the corrosion resistance of pure Zr. The mixed passive film consisting of Zr- and Mo-oxides on the metallic surface was more stable than the single passive film ZrO_2. In indirect cytotoxicity test, Zr–Mo alloys did not present significant toxic effect to L-929 fibroblast cells and MG 63 osteoblast cells, which showed an excellent *in vitro* biocompatibility. Therefore, among these experimental Zr–Mo alloys, Zr–1Mo alloy with dominant α′ phase becomes appealing when low magnetic

susceptibility and high strength (or high elastic modulus) are required for medical devices. While the β type Zr–Mo alloy shows a promising potential for new implants from the viewpoint of relatively low elastic modulus (closer to elastic modulus of natural bones).

REFERENCES

1. Sherepo K, Parfenov A, Zusmanovich I. Application of zirconium alloys to endoprostheses and osteosynthesis appliances. Biomed Eng 1992;26:238–240.
2. Thomsen P, Larsson C, Ericson LE, Sennerby L, Lausmaa J, Kasemo B. Structure of the interface between rabbit cortical bone and implants of gold, zirconium and titanium. J Mater Sci Mater Med 1997;8:653–665.
3. Niinomi M. Recent titanium R&D for biomedical applications in japan. JOM 1999;51:32–34.
4. Sherepo KM, Red'ko IA. Use of zirconium-based and zirconium-coated implants in traumatology and orthopedics. Biomed Eng 2004;38:77–79.
5. Hallab NJ, Anderson S, Caicedo M, Jacobs JJ. Zirconium and niobium affect human osteoblasts, fibroblasts, and lymphocytes in a similar manner to more traditional implant alloy metals. J ASTM Int 2006;3:429–440.
6. Guglielmotti MB, Renou S, Cabrini RL. A histomorphometric study of tissue interface by laminar implant test in rats. Int J Oral and Maxillofac Implants 1999;14:565–570.
7. Kulakov OB, Doktorov AA, Diakova SV, Denisov-Nikolskiy YI, Grötz KA. Experimental study of osseointegration of zirconium and titanium dental implants. Morfologiya 2005;127:52–55.
8. Uchida M, Kim HM, Miyaji F, Kokubo T, Nakamura T. Apatite formation on zirconium metal treated with aqueous NaOH. Biomaterials 2002;23:313–317.
9. Uchida M, Kim H-M, Kokubo T, Miyaji F, Nakamura T. Bonelike apatite formation induced on zirconia gel in a simulated body fluid and its modified solutions. J Am Ceram Soc 2001;84: 2041–2044.
10. Frandsen CJ, Brammer KS, Noh K, Connelly LS, Oh S, Chen L-H, Jin S. Zirconium oxide nanotube surface prompts increased osteoblast functionality and mineralization. Mater Sci Eng C 2011; 31:1716–1722.
11. Wang L-N, Adams A, Luo J-L. Enhancement of the capability of hydroxyapatite formation on Zr with anodic ZrO2 nanotubular arrays via an effective dipping pretreatment. J Biomed Mater Res Part B 2011;99:291–301.
12. Saldana L, Mendéz-Vilas A, Jiang L, Multigner M, González-Carrasco JL, Pérez-Prado MT, González-Martin ML, Munuera L, Vilaboa N. In vitro biocompatibility of an ultrafine grained zirconium. Biomaterials 2007;28:4343–4354.
13. Branzoi LV, Iordoc M, Codescu M. Electrochemical studies on the stability and corrosion resistance of new zirconium-based alloys for biomedical applications. Surf Interface Anal 2008;40:167–173.
14. Oliveira NTC, Biaggio SR, Rocha-Filho RC, Bocchi N. Electrochemical studies on zirconium and its biocompatible alloys Ti-50Zr at.% and Zr-2.5Nb wt.% in simulated physiologic media. J Biomed Mater Res Part A 2005;74:397–407.
15. Satpati AK, Phadnis SV, Sundaresan RI. Electrochemical and XPS studies and the potential scan rate dependent pitting corrosion behavior of Zircaloy-2 in 5% NaCl solution. Corros Sci 2005;47: 1445–1458.
16. Zhou FY, Wang BL, Qiu KJ, Lin WJ, Li L, Wang YB, Nie FL, Zheng YF. Microstructure, corrosion behavior and cytotoxicity of Zr–Nb alloys for biomedical application. Mater Sci Eng C 2012;32: 851–857.
17. Kondo R, Suyalatu, Tsutsumi Y, Doi H, Nomura N, Hanawa T. Microstructure and mechanical properties of Pt-added and Pd-added Zr-20Nb alloys and their metal release in 1 mass% lactic acid solution. Mater Sci Eng C 2011;31:900–905.
18. Bozzini B, Carlino P, Mele C. Electrochemical behaviour and surface characterisation of Zr exposed to an SBF solution containing glycine, in view of dental implant applications. J Mater Sci Mater Med 2011;22:193–200.
19. Brânzoi V, Iordoc M, Brânzoi F, Sbarcea G, Marinescu V. Surface characterization and electrochemical behavior of new biomedical Zr-based metal/ceramic composite in fetal bovine serum. Rev Roum Chim 2010;55:585–597.
20. Hobbs LW, Rosen VB, Mangin SP, Treska M, Hunter G. Oxidation microstructures and interfaces in the oxidized zirconium knee. Int J Appl Ceram Technol 2005;2:221–246.
21. Lee JKL, Maruthainar K, Wardle N, Haddad F, Blunn GW. Increased force simulator wear testing of a zirconium oxide total knee arthroplasty. Knee 2009;16:269–274.
22. Buczynski BW, Kory MM, Steiner RP, Kittinger TA, Ramsier RD. Bacterial adhesion to zirconium surfaces. Colloids Surf B 2003;30: 167–175.
23. Bui FM, Bott K, Mintchev MP. A quantitative study of the pixel-shifting, blurring and nonlinear distortions in MRI images caused by the presence of metal implants. J Med Eng Technol 2000;24: 20–27.
24. Shafiei F, Honda E, Takahashi H, Sasaki T. Artifacts from dental casting alloys in magnetic resonance imaging. J Dent Res 2003; 82:602–606.
25. Nomura SN, Oya K, Tanaka Y, Kondo R, Doi H, Tsutsumi Y, Hanawa T. Microstructure and magnetic susceptibility of as-cast Zr–Mo alloys. Acta Biomater 2010;6:1033–1038.
26. Suyalatu, Kondo R, Tsutsumi Y, Doi H, Nomura N, Hanawa T. Effects of phase constitution on magnetic susceptibility and mechanical properties of Zr-rich Zr–Mo alloys. Acta Biomater 2011;7: 4259–4266.
27. Kondo R, Nomura SN, Tsutsumi Y, Doi H, Hanawa T. Microstructure and mechanical properties of as-cast Zr–Nb alloys. Acta Biomater 2011;7:4278–4284.
28. Okazaki Y, Rao S, Asao S, Tateishi T. Effects of metallic concentrations other than Ti, Al and V on cell viability. Mater Trans JIM 1998;39:1070–1079.
29. Northwood DO. Heat treatment, transformation reactions and mechanical properties of two high strength zirconium alloys. J Less-Common Met 1978;61:199–212.
30. Hsu H-C, Wu S-C, Sung Y-C, Ho W-F. The structure and mechanical properties of as-cast Zr–Ti alloys. J Alloys Compd 2009;488: 279–283.
31. Kokubo T, Takadama H. How useful is SBF in predicting in vivo bone bioactivity? Biomaterials 2006;27:2907–2915.
32. ISO-10993-5. Biological evaluation of medical devices-part 5: Test for in vitro cytotoxicity. Arlington, VA: ANSI/AAMI;1999.
33. Slater JC. Atomic Radii in Crystals. J Chem Phys 1964;41: 3199–3204.
34. Ho W-F, Chiang T-Y, Wu S-C, Hsu H-C. Mechanical properties and deformation behavior of cast binary Ti–Cr alloys. J Alloys Compd 2009;468:533–538.
35. Mareci D, Chelariu R, Gordin D-M, Ungureanu G, Gloriant T. Comparative corrosion study of Ti–Ta alloys for dental applications. Acta Biomater 2009;5:3625–3639.
36. Davydov AD. Breakdown of valve metal passivity induced by aggressive anions. Electrochim Acta 2001;46:3777–3781.
37. Botstein O, Talianker M, Rabinkin A. Diffusionless omega transformations in quenched and pressurized Zr–Mo alloys. Acta Metall 1983;31:947–953.
38. Song S, Gray G. Influence of temperature and strain rate on slip and twinning behavior of Zr. Metall Mater Trans A 1995;26: 2665–2675.
39. Lee CM, Ju CP, Chern Lin JH. Structure–property relationship of cast Ti–Nb alloys. J Oral Rehabil 2002;29:314–322.
40. Ho W-F, Wu S-C, Hsu S-K, Li Y-C, Hsu H-C. Effects of molybdenum content on the structure and mechanical properties of as-cast Ti–10Zr-based alloys for biomedical applications. Mater Sci Eng C 2012;32:517–522.
41. Stewart TD, Hall RM. Basic biomechanics of human joints: Hips, knees and the spine. Curr Orthop 2006;20:23–31.
42. Huiskes R. The various stress patterns of press-fit, ingrown,and cemented femoral stems. Clin Orthop 1990;261:27–38.
43. Roy ME, Whiteside LA, Xu J, Katerberg BJ. Diamond-like carbon coatings enhance the hardness and resilience of bearing surfaces for use in joint arthroplasty. Acta Biomater 2010;6:1619–1624.

44. Niinomi M, Nakai M. Titanium-based biomaterials for preventing stress shielding between implant devices and bone. Int J Biomater 2011;2011:1–10.
45. Tsutsumi Y, Takano Y, Doi H, Noda K, Hanawa T. Corrosion behavior of zirconium based alloys in simulated body fluids. Mater Sci Forum 2007;561–565:1489–1492.
46. Palit GC, Gadiyar HS. Pitting corrosion of zirconium in chloride solution. Corrosion 1987;43:140–148.
47. Oliveira NTC, Guastaldi AC. Electrochemical behavior of Ti–Mo alloys applied as biomaterial. Corros Sci 2008;50:938–945.
48. Oliveira NTC, Guastaldi AC, Piazza S, Sunseri C. Photo-electrochemical investigation of anodic oxide films on cast Ti–Mo alloys. I. Anodic behaviour and effect of alloy composition. Electrochim Acta 2009;54:1395–1402.
49. Eisenbarth E, Velten D, Müller M, Thull R, Breme J. Biocompatibility of beta-stabilizing elements of titanium alloys. Biomaterials 2004;25:5705–5713.
50. Liu L, Qiu CL, Chen Q, Chan KC, Zhang SM. Deformation behavior, corrosion resistance, and cytotoxicity of Ni-free Zr-based bulk metallic glasses. J Biomed Mater Res Part A 2008; 86:160–169.
51. Yun YH, Turitto VT, Daigle KP, Kovacs P, Davidson JA, Slack SM. Initial hemocompatibility studies of titanium and zirconium alloys: Prekallikrein activation, fibrinogen adsorption, and their correlation with surface electrochemical properties. J Biomed Mater Res 1996;32:77–85.
52. Vyskocil A, Viau C. Assessment of molybdenum toxicity in humans. J Appl Toxicol 1999;19:185–192.
53. Niinomi M. Recent research and development in titanium alloys for biomedical applications and healthcare goods. Sci Technol Adv Mater 2003;4:445–454.
54. Lugowski SJ, Smith DC, McHugh AD, Van Loon JC. Release of metal ions from dental implant materials in vivo: Determination of Al, Co, Cr, Mo, Ni, V, and Ti in organ tissue. J Biomed Mater Res 1991;25:1443–1458.
55. Hallab NJ, Anderson S, Caicedo M, Brasher A, Mikecz K, Jacobs JJ. Effects of soluble metals on human peri-implant cells. J Biomed Mater Res Part A 2005;74:124–140.